Journal of Electronic Materials (2023) 52:7164–7170
https://doi.org/10.1007/s11664-023-10651-z

ORIGINAL RESEARCH ARTICLE

# Crystal Structure, Sintering Behavior, and Microwave Dielectric Properties of Low-Permittivity $Ba_2Zr_2Si_3O_{12}$ Ceramics

**Yingxiang Li[1] · Deyin Liang[1] · Xing Zhang[2] · Zhe Xiong[2] · Bin Tang[3] · Feng Si[3] · Zixuan Fang[3] · Hao Li[4] · Zitao Shi[3] · Jingjing Chen[3]**

Received: 21 June 2023 / Accepted: 26 July 2023 / Published online: 16 August 2023


## Abstract

This study presents the dielectric properties of $Ba_2Zr_2Si_3O_{12}$ ceramics, synthesized using the solid state method. The cubic crystal structure of $Ba_2Zr_2Si_3O_{12}$ ceramics was conclusively verified through the analysis of XRD patterns and subsequent structural refinement. Refined lattice parameters of $a=b=c=10.23178$ Å were found, with a corresponding unit cell volume of $V=1071.159026$ Å$^3$. The grain microstructure of the ceramics was characterized using SEM, which showed density of 97.6% for the $Ba_2Zr_2Si_3O_{12}$ ceramic. The Si-O bond valences ($V_{Si\text{-}O}$) were found to be closely related to the $\tau_f$ of the $Ba_2Zr_2Si_3O_{12}$ ceramics. The microwave dielectric properties of the $Ba_2Zr_2Si_3O_{12}$ ceramics sintered at 1490°C were ascertained to be $\varepsilon_r=15.08$, $Q\times f=14885$ GHz ($f=9.9$ GHz), and $\tau_f=-78.6$ ppm/°C.

**Keywords** $Ba_2Zr_2Si_3O_{12}$ · cubic structure · microwave dielectric properties

## Introduction

Microwave dielectric ceramics play a crucial role in communication technology as essential components in microwave electronics. These ceramics are commonly employed as resonators, filters, and substrates in integrated circuits.[1,2] They possess three key parameters: an appropriate dielectric constant, a high quality factor, and a stable temperature coefficient of resonant frequency.[3–5] The demand for dielectric materials with reduced size, high-frequency capability, and robust thermal stability has become increasingly urgent. Hence, there is a pressing need to investigate and produce dielectric substrates with enhanced performance. A high dielectric constant can effectively reduce the device's volume, but it simultaneously generates more heat within the integrated circuit. Conversely, a low dielectric constant can decrease the signal transmission delay, with the delay time being proportional to the dielectric constant.[6,7] Moreover, it can increase the operating rate, thereby minimizing system energy losses. A higher quality factor can significantly improve the frequency selectivity, which is particularly critical in filters requiring precise frequency discrimination.[8–10] In summary, materials featuring a low dielectric constant, high quality factor, and excellent thermal stability are the optimal choice for high-frequency electronic components.

Microwave ceramics with low dielectric constant have attracted the attention of many scholars because low dielectric constant can reduce signal delay. Li et al.[11] studied a $Li_4WO_5$ ceramic with rock salt structure, and the crystal phase changed from cubic to orthorhombic at 700°C. $Ba_2MgWO_6$ ceramics with a double perovskite structure were discovered by Wang et al.[12] The relative dielectric constant calculated based on the Fourier transform infrared (FTIR) spectrum is close to the measured value, which is about 16. Wu et al.[13] found a spinel structure of $MgGa_2O_4$ ceramics, which not only has a low dielectric constant, but also has a $\tau_f$ value near zero. Jiang et al.[14] studied a rock salt structure $Li_5ZnSnNbO_8$ ceramic with space group Fm-3 m, which

✉ Yingxiang Li
408960349@qq.com

1 College of Information Engineering, Shaoyang University, Shaoyang 422000, China

2 Sichuan Province Key Laboratory of Information Materials and Devices Application, College of Optoelectronic Engineering, Chengdu University of Information Technology, Chengdu 610225, China

3 State Key Laboratory of Electronic Thin Films and Integrated Devices, University of Electronic Science and Technology of China, Chengdu 611731, China

4 College of Electrical and Information Engineering, Hunan University, Changsha 410082, China

has high density and good microwave properties ($\varepsilon_r = 17.17$, $Q \times f = 51519$ GHz and $\tau_f = -28.2$ ppm/°C). In recent years, microwave ceramics based on Si and Ge have garnered significant attention from researchers owing to their exceptional microwave dielectric properties. For instance, Zou et al. reported the discovery of an anti-reductive ceramic, $Ba_2ZnSi_2O_7$ ($Q \times f = 27200$ GHz), [15] exhibiting low dielectric loss. Du et al. investigated an orthorhombic microwave ceramic, $Li_4SrCaSi_2O_8$ ($Q \times f = 90094$ GHz),[16] which demonstrated a high quality factor. Additionally, cubic microwave ceramics generally exhibit low dielectric loss, exemplified by $Li_2ZnGe_3O_8$ ($Q \times f = 47400$ GHz),[17] $Li_4Mg_2NbO_6F$ ($Q \times f = 93300$ GHz),[18] $Li_4NbO_4F$ ($Q \times f = 61{,}111$ GHz),[19] and $Li_5GaO_8$ ($Q \times f = 127040$ GHz).[20]

In this study, we focus on the investigation of a novel microwave ceramic, $Ba_2Zr_2Si_3O_{12}$, synthesized by the traditional solid-state method. The microwave dielectric properties of $Ba_2Zr_2Si_3O_{12}$ ceramics are thoroughly explored. The crystal structure of $Ba_2Zr_2Si_3O_{12}$ ceramics is characterized using x-ray diffraction (XRD) analysis and subsequent refinement. Overall, $Ba_2Zr_2Si_3O_{12}$ ceramics with reduced dielectric loss exhibit promising potential as dielectric materials.

## Experimental Procedure

$Ba_2Zr_2Si_3O_{12}$ ceramics were synthesized via the traditional solid-state method. High-purity raw materials, including $BaCO_3$ (99%, Aladdin), $ZrO_2$ (99%, Aladdin), and $SiO_2$ (99%, Aladdin), were precisely weighed according to the chemical formula ratio. Table I shows the quantity of raw materials used. The resulting powder mixture was subjected to ball milling for 8 h, utilizing alcohol as the milling medium. Subsequently, the obtained slurry was dried in an electric furnace and calcined at 1300°C for 4 h. The same process was used to produce the dried powder. The dried powder was mixed with an appropriate amount of poly(vinyl alcohol) (PVA) binder and pressed under pressure of 20 MPa to form several white cylindrical specimens. These specimens were sintered in air at temperatures ranging from 1430°C to 1510°C for 4 h. The sintered sample was thermally etched for 30 min at 50°C below the sintering temperature after polishing.

The density of the $Ba_2Zr_2Si_3O_{12}$ samples was measured using the Archimedes principle. The sample was placed into the upper tray to obtain the mass of the sample in air. Then the sample was put into the lower container, and the mass of the sample in water was obtained after complete invasion of water. Finally, the density of the sample was calculated. To investigate the phase structure of the $Ba_2Zr_2Si_3O_{12}$ ceramics, XRD analysis was performed. The XRD data of the samples were refined using GSAS software. The microstructure of the $Ba_2Zr_2Si_3O_{12}$ ceramics was investigated using scanning electron microscopy (SEM) with a Hitachi SU1510 microscope (Hitachi, Japan). The key microwave dielectric properties, namely the relative dielectric constant ($\varepsilon_r$), quality factor ($Q \times f$), and temperature coefficient of resonant frequency ($\tau_f$), were ascertained using the Hakki–Coleman dielectric resonator technique. When taking $\tau_f$ measurements, a high- and low-temperature test chamber was employed, with a temperature range of 25°C through 85°C. The $\tau_f$ value was computed using the following equation:

$$\tau_f = \frac{\Delta f}{f_0 \times \Delta t} \times 10^6 = \frac{f_{85} - f_{25}}{f_{25} \times (85-25)} \times 10^6 (\text{ppm}/^\circ\text{C}) \quad (1)$$

**Table I** Chemical materials for preparing $Ba_2Zr_2Si_3O_{12}$ ceramics

| Material | $BaCO_3$ | $ZrO_2$ | $SiO_2$ |
|---|---|---|---|
| Mass | 26.8382 g | 16.7579 g | 12.2563 g |

## Results and Discussion

The XRD pattern of the $Ba_2Zr_2Si_3O_{12}$ samples sintered at temperatures of 1430–1510°C is presented in Fig. 1. The XRD results demonstrate that the samples calcined within this temperature range exhibit consistent patterns and align well with the standard PDF card (ICDD #00-025-1466), confirming the crystal phase to be $Ba_2Zr_2Si_3O_{12}$ without any impurity phases. To further analyze the crystal structure, the XRD data of the sample were refined using the $K_2Mg_2S_3O_{12}$ compound, which shares the same structure as $Ba_2Zr_2Si_3O_{12}$. Figure 2a exhibits the refinement of the XRD data for $Ba_2Zr_2Si_3O_{12}$ sintered at 1490°C, demonstrating good agreement between the simulated and experimental

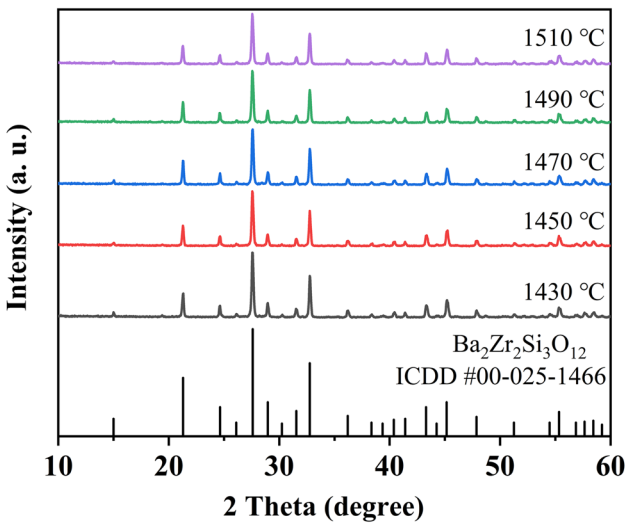


**Fig. 1** XRD patterns of $Ba_2Zr_2Si_3O_{12}$ ceramics calcined at 1430–1510°C.

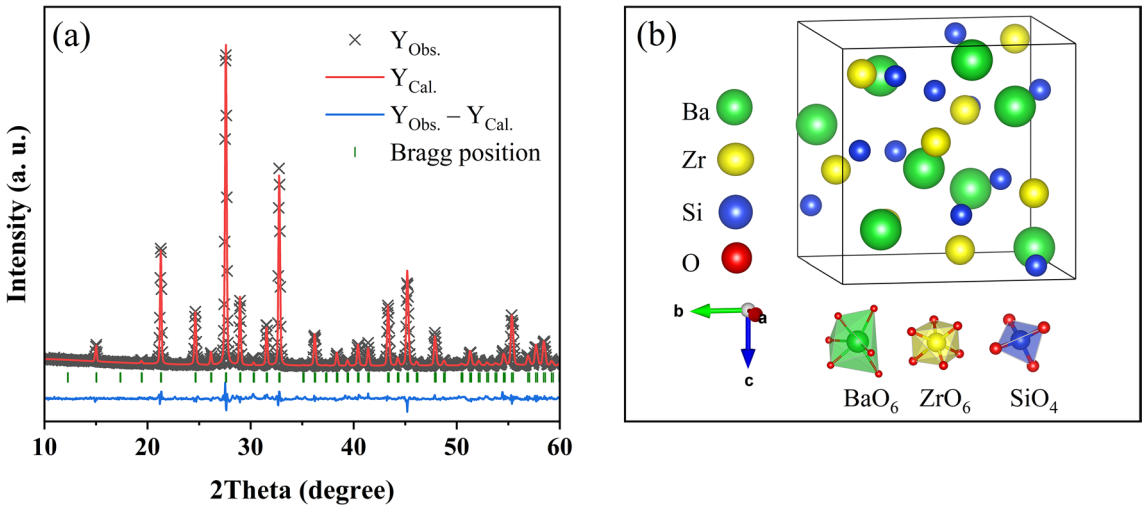


**Fig. 2** (a) Refined spectra of $Ba_2Zr_2Si_3O_{12}$ calcined at 1490°C and (b) corresponding crystal structure.

**Table II** Refinement of XRD data for $Ba_2Zr_2Si_3O_{12}$ samples

| S.T. (°C) | 1430 | 1450 | 1470 | 1490 | 1510 |
|---|---|---|---|---|---|
| $a=b=c$ (Å) | 10.23539 | 10.22607 | 10.25192 | 10.23178 | 10.22879 |
| $\alpha=\beta=\gamma$ (°) | 90 | 90 | 90 | 90 | 90 |
| V (Å$^3$) | 1072.291905 | 1069.365012 | 1077.495518 | 1071.159026 | 1070.220608 |
| $R_{wp}$ (%) | 11.06 | 10.15 | 10.74 | 10.20 | 10.27 |
| $R_p$ (%) | 7.92 | 7.27 | 7.70 | 7.29 | 7.41 |
| $\chi^2$ | 6.978 | 5.319 | 5.871 | 4.705 | 4.782 |

S.T., sintering temperature

data. The refinement results of the $Ba_2Zr_2Si_3O_{12}$ ceramics are summarized in Table II. The $R_{wp}$ and $R_p$ values at various temperatures are both less than 15%, with $R_p < R_{wp}$.[21] This finding further confirms the cubic structure of $Ba_2Zr_2Si_3O_{12}$, belonging to the P123 (198) space group. The atomic coordinates and occupation fractions of the $Ba_2Zr_2Si_3O_{12}$ ceramics are listed in Table III. Figure 2b shows the crystal structure of the $Ba_2Zr_2Si_3O_{12}$ ceramics, where a unit cell consists of four $Ba_2Zr_2Si_3O_{12}$ chemical formulas, eight $BaO_6$ octahedra, eight $ZrO_6$ octahedra, and 12 $SiO_4$ tetrahedra, with each atom occupying a specific position. The Ba and Zr atoms are situated at 4a sites, while the Si and O atoms are located at 12b positions.

**Table III** Atomic coordinates and occupation fraction of $Ba_2Zr_2Si_3O_{12}$

| Atom | $x$ | $y$ | $z$ | Occupancy | Uiso |
|---|---|---|---|---|---|
| Ba1 | 0.56800 | 0.56800 | 0.56800 | 1 | 0.03505 |
| Ba2 | 0.79700 | 0.79700 | 0.79700 | 1 | 0.01040 |
| Zr1 | 0.08400 | 0.08400 | 0.08400 | 1 | 0.03215 |
| Zr2 | 0.35000 | 0.35000 | 0.35000 | 1 | 0.02186 |
| Si | 0.03300 | 0.26800 | 0.37500 | 1 | 0.08747 |
| O1 | 0.01200 | 0.19600 | 0.24600 | 1 | 0.30848 |
| O2 | 0.17300 | 0.25800 | 0.42700 | 1 | 0.02476 |
| O3 | 0.02100 | 0.05700 | 0.71300 | 1 | 0.04969 |
| O4 | 0.00200 | 0.41200 | 0.34900 | 1 | 0.00866 |

SEM images of the polished and thermally etched cross-sections and grain size distribution of the samples sintered at 1430–1510°C are presented in Figs. 3 and 4, respectively. As the sintering temperature increases, the average grain size of the sample continues to increase. At a calcination temperature of 1430°C, the sample exhibits a higher presence of pores between the grains, with an average grain size of 2.70 μm. Despite the presence of some pores, the sample sintered at the optimal temperature of 1490°C achieves a relative density of 97.6%. In addition, the average grain size of the sample is 4.03 μm. However, at 1510°C, the grain size of the sample increases dramatically, reaching an average size of 4.37 μm.[22] Additionally, the sample exhibits a greater number of pores and poorer morphological quality due to the higher temperature employed.

Figure 5a illustrates the variation in relative density as a function of temperature for the $Ba_2Zr_2Si_3O_{12}$ samples. The relative density increases from 90.4% to 96.1% as the temperature increases from 1430°C to 1470°C, reaches

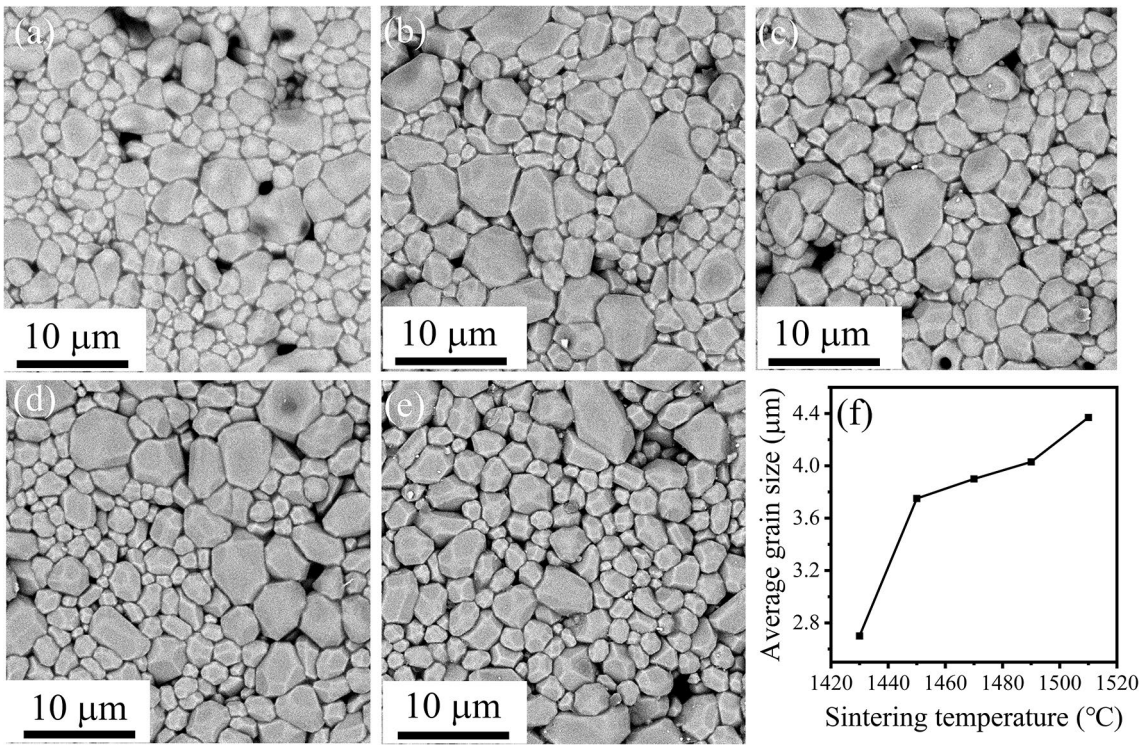


**Fig. 3** SEM images of $Ba_2Zr_2Si_3O_{12}$ ceramics calcined at various temperatures, (a) 1430°C, (b) 1450°C, (c) 1470°C, (d) 1490°C, and (e) 1510°C, for 4 h.

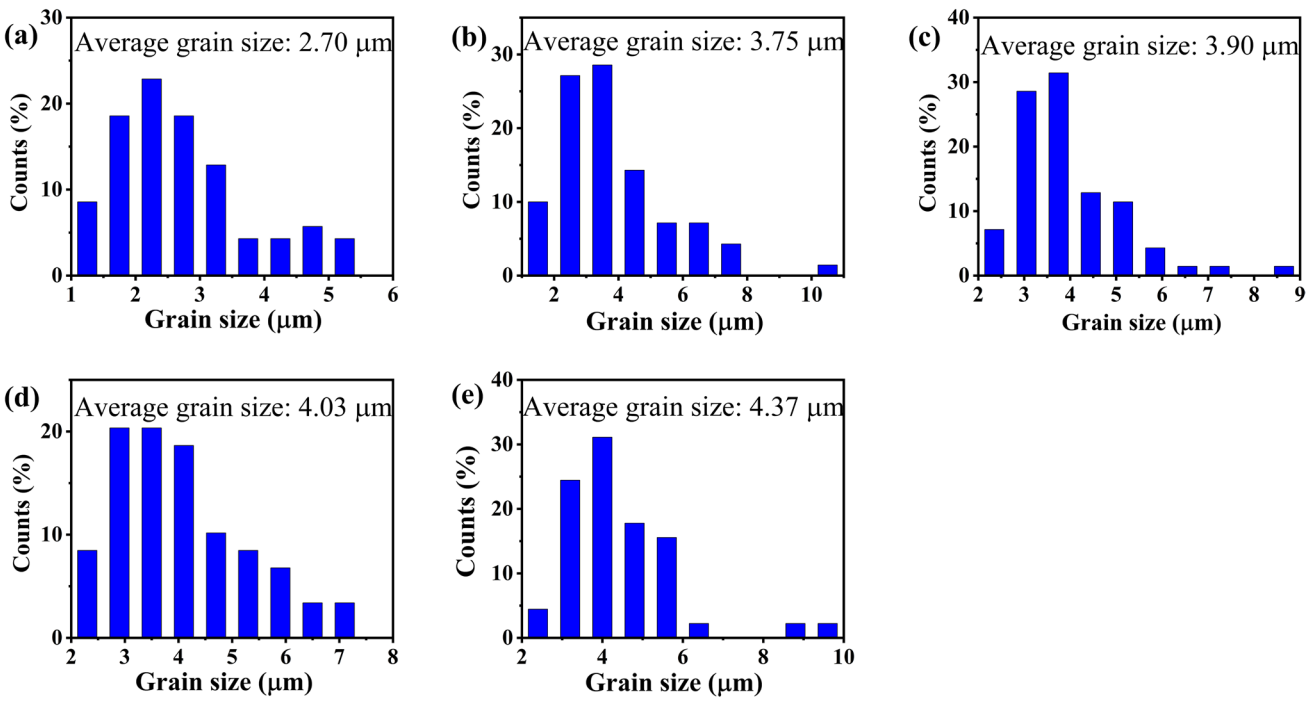


**Fig. 4** Grain size distribution and average grain size analysis of $Ba_2Zr_2Si_3O_{12}$ ceramics calcined at different temperatures: (a) 1430°C, (b) 1450°C, (c) 1470°C, (d) 1490°C, and (e) 1510°C.

its maximum value at 1490°C (97.6%), and subsequently exhibits a slight decrease. The temperature-dependent curve of the relative dielectric constant is shown in Fig. 5b. $Ba_2Zr_2Si_3O_{12}$ ceramics exhibit a peak value of 15.08 at 1490°C and a minimum value of 13.72 at 1430°C. The observed trend indicates an initial increase followed by a decrease in the $\varepsilon_r$ value with temperature. $\varepsilon_r$ is influenced by various factors, including density, ionic polarizability, porosity, molecular volume, and the presence of secondary phases. The lower $\varepsilon_r$ value of $Ba_2Zr_2Si_3O_{12}$ ceramics can be attributed to the low ionic polarizability of $Zr^{4+}$ ($\alpha = 3.25$ Å$^3$) and $Si^{4+}$ ($\alpha = 0.87$ Å$^3$) ions.[23] XRD and SEM analyses confirm the absence of apparent secondary phases in $Ba_2Zr_2Si_3O_{12}$ ceramics, indicating that secondary phases do not contribute significantly to the observed dielectric behavior. The relationship between the porosity-corrected dielectric constant ($\varepsilon_{corr}$) and $\varepsilon_r$ can be expressed as:[24]

$$\varepsilon_{corr} = \varepsilon_r(1 + 1.5p) \quad (2)$$

where $p$ represents porosity. The $\varepsilon_{corr}$ value of $Ba_2Zr_2Si_3O_{12}$ ceramics sintered at 1490°C is measured to be 15.62, slightly higher than the experimental value. The molecular volume is expected to vary inversely with the $\varepsilon_r$ value;[25] however, the observed changes in the crystal volume of $Ba_2Zr_2Si_3O_{12}$ ceramics reported in Table II do not conform to this relationship. For instance, the sample sintered at 1470°C exhibits a larger unit cell volume than that sintered at 1450°C, while displaying an increasing trend in $\varepsilon_r$. This behavior can be attributed to the corresponding increase in the relative density of the sample. Similarly, the sample sintered at 1510°C shows a slightly smaller cell volume than that sintered at 1490°C, but the $\varepsilon_r$ value decreases slightly, likely due to a decrease in relative density.

The temperature dependence of $Q \times f$ and packing fraction of $Ba_2Zr_2Si_3O_{12}$ ceramics is presented in Fig. 5c. $Q \times f$ is influenced by various factors including densification, impurities, secondary phases, crystal structure, and packing fraction. The $Q \times f$ value achieves a maximum of 14,885 GHz at 1490°C. Prior to 1490°C, the $Q \times f$ value presents an increasing trend with temperature, followed by a decrease at 1510°C (14,195 GHz). The packing fraction of $Ba_2Zr_2Si_3O_{12}$ ceramics can be calculated using the following equation:[26]

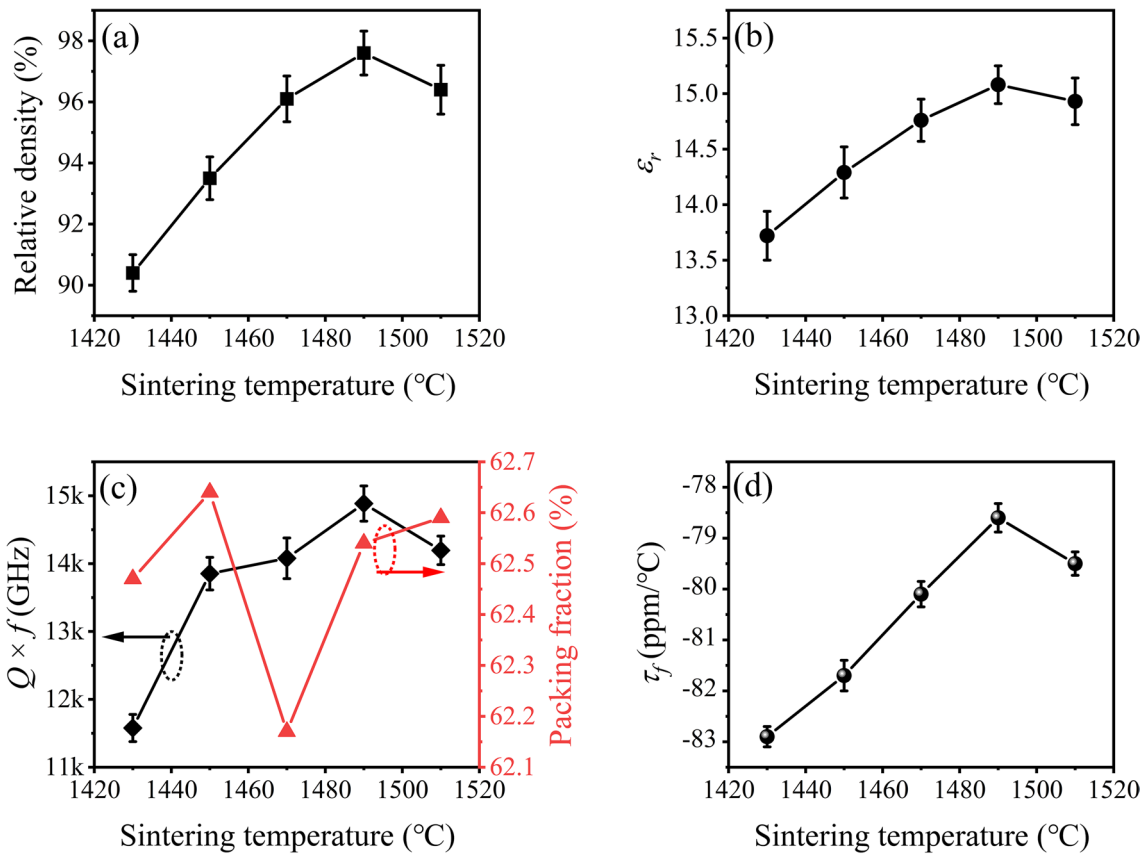


**Fig. 5** Variation curves depicting the properties of $Ba_2Zr_2Si_3O_{12}$ ceramics at different temperatures: (a) relative density, (b) $\varepsilon_r$, (c) $Q \times f$ and packing fraction, and (d) $\tau_f$.

$$\text{packing fraction}(\%) = \frac{\text{volume of the atoms in the cell} \times Z}{\text{volume of the unit cell}} \quad (3)$$

where $Z$ represents the number of $Ba_2Zr_2Si_3O_{12}$ chemical formula units in the unit cell, with a value of 4 for $Ba_2Zr_2Si_3O_{12}$ ceramics. The packing fraction of $Ba_2Zr_2Si_3O_{12}$ ceramics calcined at 1490°C is calculated to be 62.54%. A higher packing fraction corresponds to weaker lattice vibration, resulting in lower dielectric loss, thus showing a positive correlation with $Q\times f$. However, it is observed that the packing fraction is inversely proportional to the $Q\times f$ value when the sample is calcined between 1450 and 1470°C. Importantly, the $Q\times f$ value displays a similar trend as the relative density, suggesting a significant influence of density on the $Q\times f$ of $Ba_2Zr_2Si_3O_{12}$ ceramics. The decrease in relative density at 1510°C is identified as a major cause for the deterioration of $Q\times f$.

Figure 5d displays the relationship between $\tau_f$ and temperature for $Ba_2Zr_2Si_3O_{12}$ ceramics. The $\tau_f$ value of $Ba_2Zr_2Si_3O_{12}$ ceramics reaches a maximum of −78.6 ppm/°C at 1490°C, gradually increasing from 1430°C to 1470°C, and then decreasing to −79.5 ppm/°C at 1510°C. The $\tau_f$ is closely connected to the bond valence of chemical bonds. The bond valence of $Ba_2Zr_2Si_3O_{12}$ ceramics can be calculated using the following formulas:[27]

$$V_{ij} = \sum v_{ij} \quad (4)$$

$$v_{ij} = \exp\left[\frac{R_{ij} - d_{ij}}{b}\right] \quad (5)$$

where $V_{ij}$ represents the sum of all bond valences, $d_{ij}$ represents the bond length between atoms $i$ and $j$, $R_{ij}$ represents the bond valence parameter, and $b$ is a constant with a value of 0.37. Figure 6 illustrates the variation in Si-O bond valence and $\tau_f$ for $Ba_2Zr_2Si_3O_{12}$ ceramics. Previous studies have demonstrated an inverse relationship between bond valence and $|\tau_f|$ in crystal structures.[28] The Si-O bond valences ($V_{Si\text{-}O}$) for $Ba_2Zr_2Si_3O_{12}$ ceramics sintered at 1450°C, 1470°C, and 1490°C are calculated as 4.82, 5.05, and 5.21, respectively. Therefore, the decrease in $|\tau_f|$ at 1490°C is likely attributed to the increase in bond valence. Similarly, the increase in $|\tau_f|$ at 1510°C can be attributed to a decrease in bond valence. As depicted in the figure, the change in $\tau_f$ is not significant, which may be attributed to the absence of secondary phases and the insensitivity of $Ba_2Zr_2Si_3O_{12}$ ceramic material to temperature variations.[29] Figure 7 shows the variation curves of $\varepsilon_r$ and tan $\delta$ of the samples sintered at 1430–1510°C. $\varepsilon_r$ and tan $\delta$ have the opposite trend, and tan δ first decreases and then increases. When the sintering temperature is 1430–1490°C, tan $\delta$ falls from 8.55 to the lowest point 6.65, and $\varepsilon_r$ of the sample has

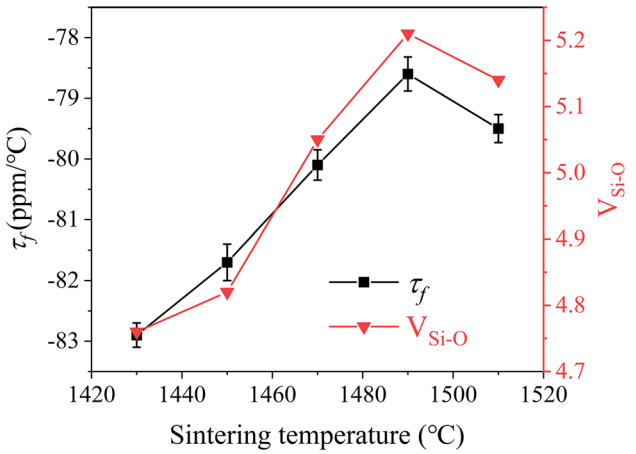


**Fig. 6** The relationship between $\tau_f$ and $V_{Si\text{-}O}$ of the samples at different temperatures.

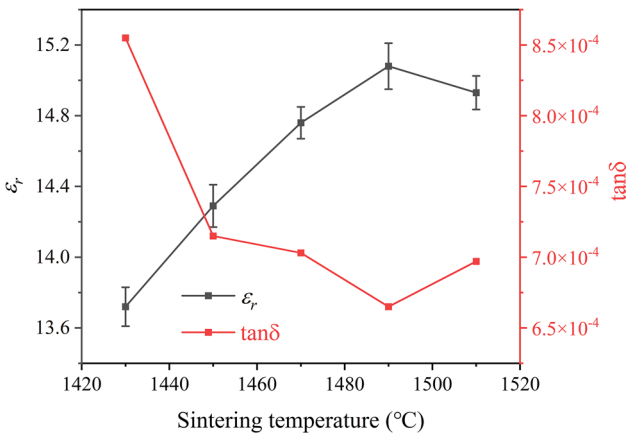


**Fig. 7** The variation curves of $\varepsilon_r$ and tan $\delta$ with sintering temperature.

a maximum value of 15.08. The tan $\delta$ of the sample sintered at 1510°C rises slightly, and $\varepsilon_r$ declines to 14.93, which may be attributed to the decrease in the relative density of the sample.

## Conclusion

In this study, we successfully synthesized a $Ba_2Zr_2Si_3O_{12}$ ceramic by the traditional solid-state reaction method and considered its microwave properties. Through XRD and Rietveld refinement analysis, we determined that the optimal sintering temperature range for achieving a pure cubic $Ba_2Zr_2Si_3O_{12}$ ceramic is 1430–1510°C. SEM images confirmed the uniformity and denseness of the sample grains when sintered at 1490°C. The microwave dielectric properties of the $Ba_2Zr_2Si_3O_{12}$ ceramics calcined at 1490°C for 4 h were as follows: $\varepsilon_r = 15.08$, $Q\times f = 14{,}885$ GHz

($f$ = 9.9 GHz), and $\tau_f$ = −78.6 ppm/°C. These results highlight the low loss and low dielectric constant characteristics of the $Ba_2Zr_2Si_3O_{12}$ ceramic, positioning it as a highly promising material for microwave dielectric ceramics applications.

**Acknowledgments** This work was supported by the graduate scientific research innovation project of Shaoyang University (Grant No. CX2022SY035) and the National Natural Science Foundation of China (Grant No. 52102123).

**Conflict of interest** The authors declare that they have no known competing financial interests or personal relationships that could have appeared to influence the work reported in this paper.

## References

1. J. Zhang, R. Zuo, and Y. Cheng, Relationship of the structural phase transition and microwave dielectric properties in $MgZrNb_2O_8$–$TiO_2$ ceramics. *Ceram. Int.* 42, 7681 (2016).
2. F. Li, Y. Li, Y. Li, X. Feng, J. Zhang, X. Liu, Y. Lu, S. Wang, Y. Liao, T. Tang, and Q. Wen, Enhanced $Na^+$-substituted $Li_2Mg_2Mo_3O_{12}$ ceramic substrate based on ultra-low temperature co-fired ceramic technology for microwave and terahertz polarization-selective functions. *J. Eur. Ceram. Soc.* 43, 384 (2023).
3. C. Dong, H. Wang, T. Yan, J. Zhao, J. Xu, and D. Wang, The influence of $CaF_2$ doping on the sintering behavior and microwave dielectric properties of CaO-$B_2O_3$-$SiO_2$ glass-ceramics for LTCC applications. *Crystals* 13(5), 748 (2023).
4. S. Li, C. Li, M. Mao, K. Song, Y. Iqbal, A. Khesro, S.S. Faouri, Z. Lu, B. Liu, S. Sun, and D. Wang, High Q×f values of Zn-Ni co-modified $LiMg_{0.9}Zn_{0.1-x}Ni_xPO_4$ microwave dielectric ceramics for 5G/6G LTCC modules. *J. Eur. Ceram. Soc.* 42(13), 5684 (2022).
5. T. Yan, C. Dong, J. Zhao, A. Khesro, Z. Liu, S. Sun, J. Li, R. Sun, and D. Wang, Lead-free borosilicate glass/fused quartz composites for LTCC applications. *J. Mater. Sci. Mater. Electron.* 33(18), 15033 (2022).
6. W. Bian, G. Zhou, Y. Dong, X. Lu, H. Zhu, S. Ta, L. Wang, and Q. Zhang, Structural analysis and microwave dielectric properties of a novel $Li_2Mg_2Mo_3O_{12}$ ceramic with ultra-low sintering temperature. *Ceram. Int.* 47, 7081 (2021).
7. Y. Chen, H. Li, X. Xu, Y. Zhang, J. Du, H. Wu, L. Liu, and G. Duan, Effects of $(Ba1/3Sb2/3)^{4+}$ on the structure and dielectric properties of $Ce_2Zr_3(MoO_4)_9$ ceramic at microwave frequency. *J. Alloy. Compd.* 939, 168804 (2023).
8. Z.A. Mikhaylovskaya, E.S. Buyanova, A.I. Malkin, A.N. Korotkov, N.S. Knyazev, and S.A. Petrova, Morphological and microwave dielectric properties of Bi: $SrMoO_4$ ceramic. *J. Solid State Chem.* 316, 123555 (2022).
9. L. Huang, S. Ding, X. Yan, T. Song, and Y. Zhang, Structure and microwave dielectric properties of $BaAl_2Si_2O_8$ ceramic with $Li_2O$–$B_2O_3$ sintering additive. *J. Alloy. Compd.* 820, 153100 (2020).
10. R. Gupta, E.Y. Kim, H.S. Shin, G.Y. Lee, and D.H. Yeo, Structural, microstructural, and microwave dielectric properties of $(Al_{1-x}B_x)_2Mo_3O_{12}$ ceramics with low dielectric constant and low dielectric loss for LTCC applications. *Ceram. Int.* 49, 22690 (2023).
11. J. Li, L. Fang, H. Luo, J. Khaliq, Y. Tang, and C. Li, $Li_4WO_5$: a temperature stable low-firing microwave dielectric ceramic with rock salt structure. *J. Eur. Ceram. Soc.* 36, 243 (2016).
12. Y. Wang, J. Lv, J. Wang, F. Shi, and Z. Qi, Lattice vibrational characteristics, crystal structure and dielectric properties of $Ba_2MgWO_6$ microwave dielectric ceramic. *Ceram. Int.* 47, 17784 (2021).
13. S. Wu, J. Xue, R. Wang, and J. Li, Synthesis, characterization and microwave dielectric properties of spinel $MgGa_2O_4$ ceramic materials. *J. Alloy. Compd.* 585, 542 (2014).
14. Y. Jiang, Y. Shen, J. Yang, Z. Fang, X. Zhang, P. Zhao, and B. Tang, A novel ultra-low loss ceramic $Li_3ZnSnNbO_8$ with a rock salt structure. *Mater. Chem. Phys.* 277, 125457 (2022).
15. Z.Y. Zou, K. Du, X.K. Lan, W.Z. Lu, X.C. Wang, X.H. Wang, and W. Lei, Anti-reductive characteristics and dielectric loss mechanisms of $Ba_2ZnSi_2O_7$ microwave dielectric ceramic. *Ceram. Int.* 45, 19415 (2019).
16. Q. Du, Q. Wen, L. Jiang, S. Liu, L. Ma, and H. Li, A novel low-temperature sintering microwave dielectric ceramic $Li_4SrCaSi_2O_8$ with low-ϵr and low loss. *Ceram. Int.* 49, 22617 (2023).
17. H. Xiang, L. Fang, W. Fang, Y. Tang, and C. Li, A novel low-firing microwave dielectric ceramic $Li_2ZnGe_3O_8$ with cubic spinel structure. *J. Eur. Ceram. Soc.* 37, 625 (2017).
18. S. Zhai, P. Liu, and S. Zhang, A novel high-Q oxyfluoride $Li_4Mg_2NbO_6F$ microwave dielectric ceramic with low sintering temperature. *J. Eur. Ceram. Soc.* 41, 4478 (2021).
19. X. Chu, J. Jiang, J. Wang, Y. Wu, L. Gan, and T. Zhang, A new high-$Q{\times}f$ $Li_4NbO_4F$ microwave dielectric ceramic for LTCC applications. *Ceram. Int.* 47, 4344 (2021).
20. L. Ao, Y. Tang, J. Li, W. Fang, L. Duan, C. Su, Y. Sun, L. Liu, and L. Fang, Structure characterization and microwave dielectric properties of $LiGa_5O_8$ ceramic with low-$\varepsilon_r$ and low loss. *J. Eur. Ceram. Soc.* 40, 5498 (2020).
21. G. Yao, J. Yan, J. Tan, C. Pei, P. Liu, H. Zhang, and D. Wang, Structure, chemical bond and microwave dielectric characteristics of novel $Li_3Mg_4NbO_8$ ceramics. *J. Eur. Ceram. Soc.* 41, 6490 (2021).
22. C.F. Xing, J. Bao, Y.F. Sun, J.J. Sun, and H.T. Wu, $Ba_2BiSbO_6$: A novel microwave dielectric ceramic with monoclinic structure. *J. Alloy. Compd.* 782, 754 (2019).
23. R.D. Shannon, Dielectric polarizabilities of ions in oxides and fluorides. *J. Appl. Phys.* 73, 348 (1993).
24. K. Du, C.Z. Yin, Y.B. Guo, C. Zhang, X.C. Wang, W.Z. Lu, and W. Lei, Phase transition, infrared spectra, and microwave dielectric properties of temperature-stable $CaSnSi_{1-x}Ge_xO_5$ ceramics. *Ceram. Int.* 47, 24781 (2021).
25. E.S. Kim, C.J. Jeon, and P.G. Clem, Effects of crystal structure on the microwave dielectric properties of $ABO_4$ (A = Ni, Mg, Zn and B = Mo, W) ceramics. *J. Am. Ceram. Soc.* 95, 2934 (2012).
26. X. Zhang, Z. Fang, Y. Jiang, M. Wang, S. Gee, L. Zhou, H. Yang, F. Si, P. Zhao, Z. Xiong, S. Zhang, and B. Tang, Microwave dielectric properties of a low firing and temperature stable lithium magnesium tungstate ($Li_4MgWO_6$) ceramic with a rock-salt variant structure. *J. Eur. Ceram. Soc.* 41, 171 (2021).
27. J. Li, L. Fang, H. Luo, Y. Tang, and C. Li, Structure and Microwave dielectric properties of a novel temperature stable low-firing $Ba_2LaV_3O_{11}$ ceramic. *J. Eur. Ceram. Soc.* 36, 2143 (2016).
28. W.S. Xia, L.X. Li, L.J. Ji, P. Zhang, P.F. Ning, and Q.W. Liao, Phase evolution, bond valence and microwave characterization of $(Zn_{1-x}Ni_x)Ta_2O_6$ ceramics. *Mater. Lett.* 66, 296 (2012).
29. J. Li, Y. Tang, Z. Zhang, W. Fang, L. Ao, A. Yang, L. Liu, and L. Fang, Two novel garnet $Sr_3B_2Ge_3O_{12}$ (B = Yb, Ho) microwave dielectric ceramics with low permittivity and high $Q$. *J. Eur. Ceram. Soc.* 41, 1317 (2021).